



Article

Far-Red to Near Infrared Emissive Aqueous Nanoparticles Based on a New Organic Material with Three BODIPY Dyes at the Periphery of the Core: A Combined Experimental and Theoretical Study

Benedetta M. Squeo^{1,†} , Aggelos Avramopoulos^{2,3,*}, Alkmini D. Nega⁴ , Aristeia Pavlou⁵ , Michael G. Siskos⁵, Panagiota Koralli³, Andriana Schiza³, Antonia Dimitrakopoulou-Strauss⁴, Vasilis G. Gregoriou^{1,6} and Christos L. Chochos^{1,3,*}

¹ Advent Technologies SA, Stadiou Street, Platani, Rio, 26504 Patras, Greece; benedetta.squeo@scitec.cnr.it (B.M.S.); vgregoriou@eie.gr (V.G.G.)

² Department of Physics, University of Thessaly, 35100 Lamia, Greece

³ Institute of Chemical Biology, National Hellenic Research Foundation, 48 Vassileos Constantinou Avenue, 11635 Athens, Greece; pkoralli@eie.gr (P.K.); aschiza@eie.gr (A.S.)

⁴ Clinical Cooperation Unit Nuclear Medicine, German Cancer Research Center, 69120 Heidelberg, Germany; a.negka@dkfz-heidelberg.de (A.D.N.); ads@ads-net.de (A.D.-S.)

⁵ Department of Chemistry, Section of Organic Chemistry and Biochemistry, University of Ioannina, 45110 Ioannina, Greece; aristeap.pavlou@gmail.com (A.P.); msiskos@uoi.gr (M.G.S.)

⁶ National Hellenic Research Foundation, 48 Vassileos Constantinou Avenue, 11635 Athens, Greece

* Correspondence: aavramopoulos@uth.gr (A.A.); chochos@eie.gr (C.L.C.)

† Present Address: CNR-SCITEC, Via Corti 12, 20133 Milano, Italy.



Citation: Squeo, B.M.;

Avramopoulos, A.; Nega, A.D.;

Pavlou, A.; Siskos, M.G.; Koralli, P.;

Schiza, A.; Dimitrakopoulou-Strauss,

A.; Gregoriou, V.G.; Chochos, C.L.

Far-Red to Near Infrared Emissive Aqueous Nanoparticles Based on a

New Organic Material with Three BODIPY Dyes at the Periphery of the

Core: A Combined Experimental and Theoretical Study. *Electron. Mater.*

2021, *2*, 24–38. <https://doi.org/10.3390/electronicmat2010003>

Received: 2 November 2020

Accepted: 13 January 2021

Published: 18 January 2021

Publisher's Note: MDPI stays neutral with regard to jurisdictional claims in published maps and institutional affiliations.



Copyright: © 2021 by the authors.

Licensee MDPI, Basel, Switzerland.

This article is an open access article

distributed under the terms and

conditions of the Creative Commons

Attribution (CC BY) license (<https://creativecommons.org/licenses/by/4.0/>).

Abstract: A new organic material with three 4,4-difluoro-4-borata-3a-azonia-4a-aza-s-indacene dyes (BODIPYs) at the periphery of the central core is successfully synthesized (3BDP3T) and its corresponding aqueous nanoparticles are prepared via the encapsulation approach and characterized in detail both experimentally and theoretically with the aid of the Density Functional Theory (DFT). The linear and non-linear optical properties of the synthesized material are also studied. Until now, the development of organic materials with three BODIPYs as substituents is limited and their properties are not fully resolved. The obtained 3BDP3T-based nanoparticles exhibit far-red and near infrared (NIR) emission with photoluminescence quantum yields of 0.021, which is promising as a new fluorescent contrast agent in the far-red and NIR spectral regions.

Keywords: hyperpolarizabilities; absorption spectra; DFT computations; nanoparticles; BODIPY; probe; near infrared; conjugated polymers

1. Introduction

Acceptor-Donor-Acceptor (ADA) organic electronic materials are a class of functional dyes that provided the largest impact to the field of organic electronics and, especially, the small molecule-based organic photovoltaics (OPV) materials during the last five years [1–5]. According to this concept, an electron-donating conjugated oligomer is functionalized at its ends with two electron-deficient units among which dicyanovinylene groups are the most widely utilized [6]. Stronger heterocyclic acceptors were originally utilized less frequently despite their beneficial influence on the absorption properties, i.e., reducing the band gap and increasing the color tunability.

Such a heterocyclic electron withdrawing the building block is the 4,4-difluoro-4-borata-3a-azonia-4a-aza-s-indacene dye, which is more commonly known as BODIPY. BODIPY-type dyes are an emerging class of red/near infrared (NIR) emitters (and absorbers) [7,8] because, even though the monomeric BODIPY is a green-emitting fluorophore (quantum efficiency up to 100% with narrow absorption and emission bands < 50 nm) [9], it can

be functionalized by means of a few synthetic steps so as to shift the energy gap into the NIR [10]. Discovered for the first time in 1968 by Treibs and Kreuz [11], BODIPYs are of wide importance and have a broad use as laser dyes in biological sensing, organic electronic, and other possible applications [12–17].

Taking these into account, we have recently reported the synthesis of a novel A-D-A type near infrared (NIR) organic material (referred to as NIRBDTE, for brevity, please see Figure 1 for the chemical structure) containing two BODIPY moieties as the (A) units and an oligothiophene segment as the electron donating (D) part [10]. NIRBDTE was then used as the emitter in NIR organic light emitting diodes (OLEDs) with the highest efficiency reported so far for a metal-free fluorescent material, emitting at 720 nm. Motivated by these results, we were interested in exploring alternative chemical approaches, such as going beyond the classical A-D-A type organic electronic materials, by functionalizing electron donating units with more than two BODIPY dyes for bioimaging. Organic materials with 3 BODIPYs meso substituted in the periphery of an electron donating molecule (D) are limited and their synthesis is particularly challenging. However, the development of stable meso substituted BODIPYs are the key synthetic intermediates toward higher dimensionality structures. These type of 2D or 3D organic materials are expected to provide new insights on the optical or electronic properties.

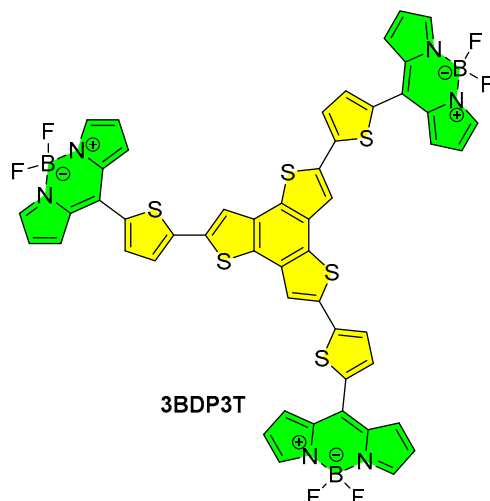


Figure 1. Chemical structure of the tri-functionalized 4,4-difluoro-4-borata-3a-azonia-4a-aza-s-indacene dyes (BODIPY) derivative.

Fluorescent probes based on small organic molecules have become fundamental tools in the science of biology due to their ability to provide information about the localization and quantity of the biological molecules without having them to be genetically modified [18]. One of the major disadvantages for the use of organic fluorophores in bioimaging is their failure to continuously fluoresce for extended periods. Moreover, most of fluorophores spectra are usually wide, which sometimes contributes to overlap of signals from numerous biological fluorophores. Therefore, between the different fluorophores, BODIPYs are the most popular group. Their efficiency of the high photostability, sharp absorption and emission patterns, high fluorescence quantum yields, and high extinction coefficients makes them perfect candidates for bioimaging [7,19].

Based on this, in this contribution, we present the successful synthesis and properties characterization of a new organic electronic material consisting of three BODIPY dyes at the periphery of the benzo[1,2-*b*:3,4-*b'*:5,6-*b''*]trithiophene (3BDP3T; Figure 1) for the first time. We manage to prepare 3BDP3T-based aqueous nanoparticles utilizing the encapsulation method and study its optical properties toward its application as far-red to near infrared (NIR) dye probe for fluorescent optical imaging. In order to shed some light on the experimental findings, a series of theoretical computations is also reported.

2. Experimental Section

2.1. Materials

All reactions are air and light sensitive and, therefore, were performed under argon and in the dark. All glassware was washed using detergent (Teepol), rinsed with excess water, acetone and methylene dichloride, and dried in an oven at 120 °C. All solvents and reagents were purchased from Aldrich. Toluene was distilled using calcium hydride (CaH₂) and benzophenone prior to polymerization. The 2,5,8-tris(trimethylstannyl)benzo[1,2-*b*:3,4-*b'*:5,6-*b''*]trithiophene was purchased from Sunatech Inc. (Suzhou, China) and 10-(5-bromothiophen-2-yl)-5,5-difluoro-5H-4λ⁴,5λ⁴-dipyrrolo[1,2-*c*:2',1'-*f*][1,3,2]diazaborinine was synthesized according to the literature [10].

Synthesis of 3BDP3T. 10-(5-bromothiophen-2-yl)-5,5-difluoro-5H-4λ⁴,5λ⁴-dipyrrolo[1,2-*c*:2',1'-*f*][1,3,2]diazaborinine (154 mg, 0.435 mmol) was mixed with the 2,5,8-tris(trimethylstannyl)benzo[1,2-*b*:3,4-*b'*:5,6-*b''*]trithiophene (100 mg, 0.136 mmol), tris(dibenzylideneacetone)dipalladium(0) (5%, 6.4 mg) and tri(*o*-tolyl)phosphine (10%, 4.1 mg) in toluene. The mixture was stirred overnight at 110 °C. The crude product was cooled down and toluene was removed under reduce pressure. The product was purified by silica gel column chromatography using a mixture of hexane:dichloromethane 7:3 eluent and then recrystallized from hexane to afford the 3BDP3T as an orange powder (80 mg, 55%). ¹H NMR (CDCl₃, 600 MHz) δ 7.96 (s, 6H), 7.58 (d, J = 3.9 Hz, 3H), 7.48 (d, J = 3.6 Hz, 3H), 7.34 (d, J = 4.21 Hz, 6H), 7.24 (s, 3H), 6.62 (d, J = 4.21 Hz, 6H).

2.2. Instrumentation

Nuclear Magnetic Resonance (NMR): ¹H-NMR measurement was carried out in solution (1% *w/v*) using CDCl₃ (Acros 99.6%) as the solvent and tetramethylsilane (TMS) as the integral standard on a Varian 600 MHz NMR spectrometer (Palo Alto, California) at an ambient temperature.

2.3. Dynamic Light Scattering (DLS)

The structural study was performed using dynamic light scattering (DLS) in order to determine the mean diameter (*d*, nm) of nanodroplets and the polydispersity index (PDI) of the system. DLS measurements were performed using the Zetasizer NanoZS device (ZEN3600) from Malvern Instruments (Malvern, UK) equipped with He-Ne (632.8 nm) laser and detection was performed at a scattering angle of 173°. The mean diameter of the dispersed nanodroplets was calculated by the Stokes-Einstein law.

$$R_H = \frac{k_B T}{6\pi\eta D} \quad (1)$$

where R_H is the hydrodynamic radii of nanodroplets, k_B is the Boltzmann constant, T is the absolute temperature, η viscosity of microemulsion (in specific temperature), and D is the diffusion constant, respectively [20].

After their preparation, the microemulsions were placed in a suitable glass cell in dust-free conditions. The experimental data were processed using version 6.32 of the Malvern Zetasizer Nano software (Malvern Panalytical Ltd., Enigma Business Park, Malvern, UK). The temperature during the measurements was constant at 25 °C. Experiments were performed in triplicate for each sample, and results were presented as an average of ± S.D.

2.4. Absorption and Photoluminescence

The absorption spectra of the tetrahydrofuran (THF) solutions and the aqueous Conjugated Polymer Nanoparticles (CPNs) were measured using a UV-Visible Analytik Jena AG Germany, Specord 205 spectrophotometer using a 1-cm path length quartz cuvette. The THF solutions were in dry conditions to prevent the stabilizers interference with the fluorescence measurement. The photoluminescence (PL) emission and the relative PL quantum yield (PLQY) was measured by PL spectroscopy when using a dilute fluorenone solution (excitation wavelength of 380 nm) in acetonitrile as the reference ($\Phi_r = 0.032$) [21,22]. The used

excitation wavelength was 520 nm. The cuvette was a 1 cm cuvette and 90°. All the fluorescence measurements were performed under argon atmosphere. A software-controlled FS5 Spectrofluorometer (Edinburgh Instruments Ltd., Livingston, UK) enabled the acquisition of photoluminescence spectra. The photoluminescence quantum yield has been calculated from the equation below [23].

$$\Phi_x = \Phi_r(F_x/F_r) \cdot (A_r/A_x) \cdot (n_x^2/n_r^2) \quad (2)$$

where,

Φ_x , is the photoluminescence quantum yield of the unknown sample,

F , is the area of the integration of the emission intensities,

n , is the refractive index of the sample and the reference,

A , is the solution optical density at the excitation wavelength.

The indexes 'r' and 'x' are referred to as the reference and the unknown sample, respectively. *Cyclic Voltammetry*: The cyclic voltammetry was conducted on a VersaSTAT4 potentiostat galvanostat with platinum (Pt) disk, Pt wire, and standard calomel electrode (SCE) as the working electrode, counter electrode, and reference electrode, respectively, using a 0.1 M-solution of tetrabutylammonium hexafluorophosphate (*n*-Bu₄NPF₆) in anhydrous acetonitrile at a potential scan rate of 50 mV s⁻¹. Thin films of samples were deposited onto the Pt disk working electrode from a chloroform solution. The potential of the SCE reference electrode was internally calibrated by using the ferrocene/ferrocenium redox couple (Fc/Fc⁺). The electrochemical energy levels were estimated by the highest occupied molecular orbital $E_{HOMO} = -[4.8 + (E_{onset}^{Ox} - Fc^{1/2})]$ and lowest unoccupied molecular orbital $E_{LUMO} = -[4.80 + (E_{onset}^{Red} - Fc^{1/2})]$.

2.5. Theoretical Calculations

We employed DFT to calculate a series of properties, the E_{HOMO} and E_{LUMO} , the first allowed electronic transition (excitation energy), the dipole moment, and the electronic (hyper)polarizabilities of 3BDP3Ta and 3BDP3Tb, both in the gas phase and in solution. In particular, E_{HOMO} and E_{LUMO} were calculated by employing a series of functionals (e.g., PBE1PBE/6-31G**, HSEH1PBE/6-311G** etc.) and their performance will be checked by using the experimental values. The computation of linear and non-linear optical response properties ((hyper)polarizabilities) will provide insights on the interaction of these derivatives with light, thus, revealing certain features associated with their structure-property relationship.

Linear and Non-Linear Optical Properties: Definitions. When a molecule is set in a uniform static electric field, F , its energy, $E(F)$, is given by:

$$E(F) = E^0 - \mu_i F_i - (1/2)\alpha_{ij} F_i F_j - (1/6)\beta_{ijk} F_i F_j F_k - (1/24)\gamma_{ijkl} F_i F_j F_k F_l - \dots, \quad (3)$$

where E^0 is the field-free energy, μ_i , α_{ij} , β_{ijk} , and γ_{ijkl} are the dipole moment, polarizability, first hyper-polarizability, and second hyper-polarizability components, respectively. A summation over repeated indices is implied. The polarizabilities and the hyper-polarizabilities are also called linear (L) and nonlinear optical (NLO) properties. The reported values for the dipole moment (μ), polarizability (α), and hyper-polarizabilities, first (β) and second (γ) are given by:

$$\mu = (\mu_x^2 + \mu_y^2 + \mu_z^2)^{1/2} \quad (4)$$

$$\alpha = \frac{1}{3}(\alpha_{xx} + \alpha_{yy} + \alpha_{zz}) \quad (5)$$

$$\sum_{i=x,y,z} \frac{\mu_i \beta_i}{\|\mu\|} \quad (6)$$

where

$$\frac{1}{5} \sum_{j=x,y,z} (\beta_{ijj} + \beta_{jij} + \beta_{jji}) \quad (7)$$

$$\gamma = \frac{1}{5} (\gamma_{xxxx} + \gamma_{yyyy} + \gamma_{zzzz} + 2\gamma_{xxyy} + 2\gamma_{xxzz} + 2\gamma_{yyzz}) \quad (8)$$

Finite field approaches [24], by employing Equation (3), have been used to compute the (hyper)polarizability components, by applying a step field of 0.001 a.u.

The Density Functional Theory computations have been performed by using the GAUSSIAN 09 software [25]. The B3LYP/6-31G* method has been employed to calculate the molecular structures we have used in this work. Vibrational analysis was performed for all structures employed in this study to verify that a stationary point has been found in the potential energy surface.

Effect of the Environment on the L&NLO Properties: We have first computed the L&NLO properties in the gas phase. The solvent effect, on the properties of interest, has been calculated by employing the Polarizable Continuum Model, which uses the integral equation formalism variant [25]. This technique employs the solute cavity via a set of overlapping spheres. Many research groups contributed to its development (e.g., Tomasi, Barone) [26,27].

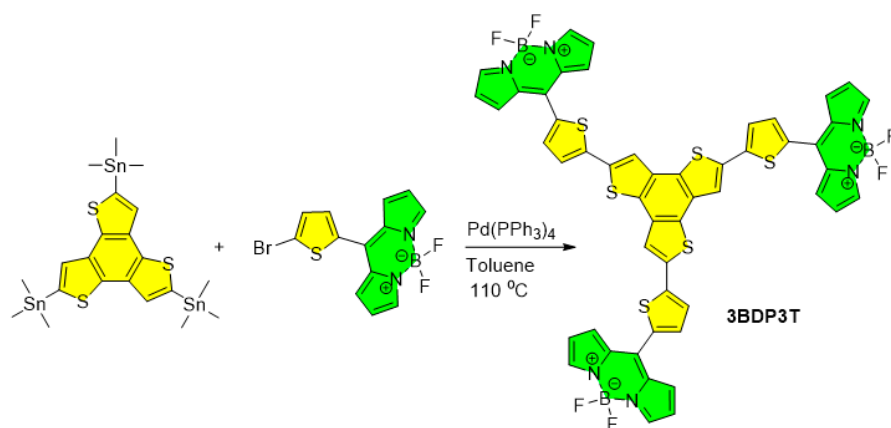
Nanoparticles Preparation: In more detail, 1 mg of 3BDP3T and 9 mg of poly(ethylene glycol) methyl ether-*block*-poly(lactide-co-glycolide) (mPEG-*b*-PLGA) were dissolved in 1 mL of THF. The choice of mPEG-*b*-PLGA was based on the fact that it is an FDA-approved and metabolizable copolymer [28]. The resulting solution is added to 7 mL of deionized water following a procedure described elsewhere [29]. The solution left overnight to allow complete evaporation of the THF and the volume of water lost was replaced. After this procedure, stable aqueous nanoparticles containing the 3BDP3T are formed. The hydrophobic PLGA segments are liable to entangle with 3BDP3T and the hydrophilic polyethylene glycol (PEG) chains should extend into the aqueous phase. The obtained nanoparticles were then filtered through a 0.2- μm cellulose acetate filter. To evaluate the sizes of the formatted aqueous nanoparticles, dynamic light scattering (DLS) measurements were performed at room temperature of 25 °C a day after their preparation.

3. Results and Discussion

3.1. Synthesis and Properties Characterization

With a view for establishing general protocols for (organic) semiconductors design, we consider that BODIPY might be an ideal acceptor end-unit because it has strong electron-withdrawing characteristics, and it is expected to provide both negative inductive (−I) effects originating from “through-bond” polarizations [10], and mesomeric (−M) effects [30], originating from π -bond polarizations. Such an approach is expected to facilitate both delocalization and stabilization of charge carriers (e.g., electrons). In practice, the development of BODIPY-based organic semiconductors and, especially those that contain more than two BODIPY units, has, so far, lagged behind that of other π -deficient units, mainly because of stability issues during the synthesis. However, thanks to a recently developed synthetic protocol, stable α,β -unsubstituted BODIPYs functionalized solely on the meso position can be successfully produced and integrated into more complex structures [10]. Following this approach, we performed a Stille cross-coupling reaction between the 10-(5-bromothiophen-2-yl)-5,5-difluoro-5H-4 λ^4 ,5 λ^4 -dipyrrolo[1,2-*c*:2',1'-*f*][1,3,2]diazaborinine and the 2,5,8-tris(trimethylstannyl)benzo[1,2-*b*:3,4-*b'*:5,6-*b''*]trithiophene to obtain the 3BDP3T (Scheme 1) that contains three BODIPY dyes at the terminal of the benzo[1,2-*b*:3,4-*b'*:5,6-*b''*] trithiophene core.

¹H-NMR analysis revealed the successful synthesis of the small molecule dyes. The BODIPY's protons (6H) were clearly observed with independent peaks at 6.65, 7.42, 7.58, and 7.98 ppm while the ratio of the integrated area between the BODIPY's and thiophenes' protons (7.24 ppm) was 2, confirming the expected structure. The UV-Visible absorption and photoluminescence spectra of 3BDP3T were recorded in tetrahydrofuran (THF) solution.



Scheme 1. Synthetic route towards the preparation of 3BDP3T.

Figure 2a shows an intense absorption peak with λ_{max} at 520 nm ($\log \epsilon = 5.28$) and an emission spectrum with λ_{max} at 630 nm and a shoulder at 680 nm. The photoluminescence quantum yield (PLQY) found 0.029 ± 0.011 from three independent measurements. This large stoke shift (c. 3300 cm^{-1}), which is considerably higher than for “normal” BODIPYs (c. 300 cm^{-1}) that is shown in 3BDP3T is desirable because we can shift the emission spectra more to the near infrared region ($>650 \text{ nm}$). Especially, the range of 1000–1700 nm (short wave infrared, SWIR) is particularly useful for bioimaging, as this electromagnetic field does not interfere with the absorption and emission of radiation due to the absorption of various biological fluids, while it is less harmful to tissues and absorption radiation at long wavelengths [31].

Cyclic voltammetry was performed to estimate the energy levels of 3BDP3T. The oxidation and reduction potentials of 3BDP3T are shown in Figure 2b. 3BDP3T exhibits reversible reduction peaks and irreversible oxidation peaks with oxidation onset potentials at 1.44 V vs. a standard calomel electrode (SCE) and -0.5 V vs. SCE, respectively, resulting in E_{HOMO} and E_{LUMO} values of -6.14 eV and -3.91 eV , respectively.

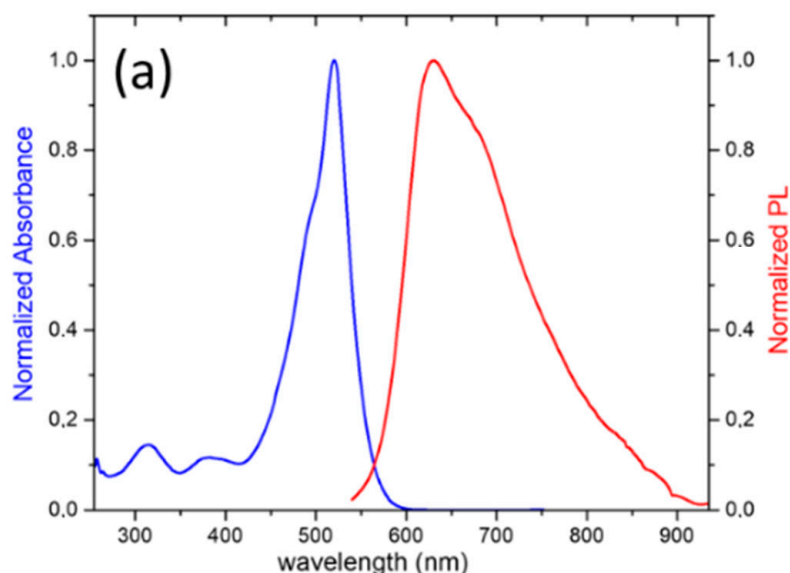


Figure 2. Cont.

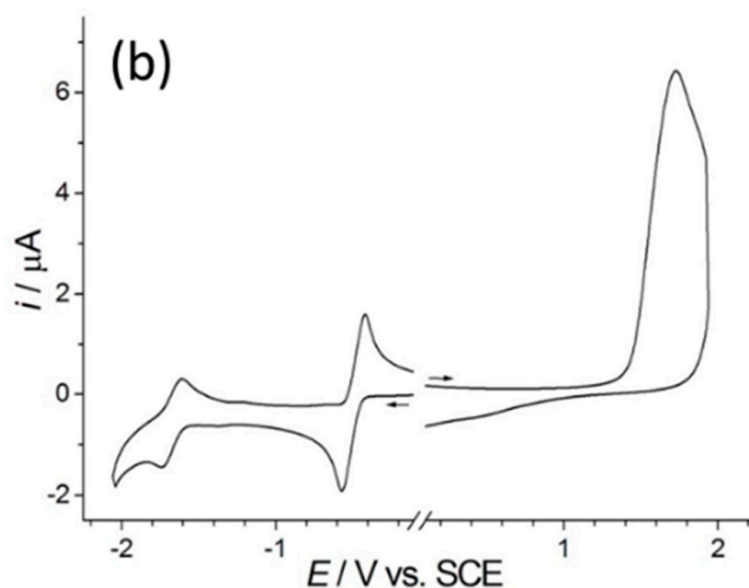


Figure 2. (a) Absorption and photoluminescence spectra (THF and excitation wavelength of 520 nm) and (b) cyclic voltammetry of 3BDP3T (0.1 M solution of tetrabutylammonium hexafluorophosphate ($n\text{-Bu}_4\text{NPF}_6$) in anhydrous acetonitrile).

3.2. Theoretical Calculations

The reported computational results will focus on: (a) the rationalization of the first absorption energy by employing Natural Transition Orbital analysis (NTO) [32], (b) the E_{HOMO} and E_{LUMO} , and the first electronic excitation energy, (c) the linear and non-linear optical properties (L&NLO) by computing the static (hyper)polarizabilities of 3BDP3Ta and 3BDP3Tb (Figure 3), (d) the effect of the solvent and small structural changes on the optical and non-linear optical properties of interest will also be discussed, and (e) the effect of BODIPY, as an electron acceptor, on the L&NLO properties, will be discussed and compared with other well-known strong electron acceptors (NO_2 , CN). Electron acceptor defines those atoms or groups that withdraw electron density [33].

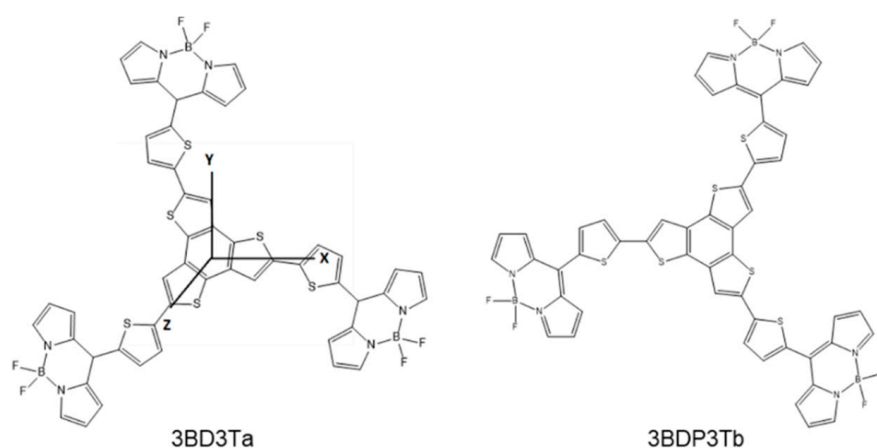


Figure 3. The two conformations of 3BDP3T reported in the present study.

Computation of E_{HOMO} and E_{LUMO} of 3BDP3Ta. In Table 1, we present the E_{HOMO} and E_{LUMO} of derivative 3BDP3Ta, computed by a series of functionals and basis sets. From these results, it is inferred that: (a) the best E_{HOMO} is given by PBE1PBE/6-31G**, B3PW91/6-311G**, (b) the best E_{LUMO} is given by HSEH1PBE/6-311G**, B3PW91/6-311G**, (c) CAM-B3LYP, B3LYP functionals overestimate the HOMO-LUMO gap, compared with the experiment. A similar trend is observed for the value computed with the MP2 method.

Therefore, it is inferred that, of all considered functionals, B3PW91/6-311G** has, apparently, the best performance when compared with the available experimental data for both E_{HOMO} and E_{LUMO} . With regard to the $E_{HOMO}-E_{LUMO}$ gap, the value which has the closest agreement with the experiment is given by the HSEH1PBE/6-311G** method.

Table 1. The E_{HOMO} , the E_{LUMO} , and the $E_{HOMO}-E_{LUMO}$ gap of 3BDP3Ta, computed in the presence of the solvent (chloroform) by employing a series of functionals and basis sets. All values are given in a.u.

Molecule ¹	E_{HOMO}	E_{LUMO}	$ E_{HOMO} - E_{LUMO} $
CAM-B3LYP/6-31G**	-0.256	-0.079	0.177
CAM-B3LYP/6-311G**	-0.263	-0.088	0.175
PBE1PBE/6-31G**	-0.223	-0.113	0.11
HSEH1PBE/6-311G**	-0.215	-0.132	0.083
B3PW91/6-311G**	-0.223	-0.125	0.098
BLYP/6-31G**	-0.180	-0.120	0.06
B3LYP/6-31G**	-0.220	-0.116	0.104
MP2/6-311G**	-0.281	-0.010	0.271
Exp. ²	-0.225	-0.144	0.081

¹ The geometry, which was employed for the computation of E_{HOMO} and E_{LUMO} and the corresponding difference, was optimized at the gas phase with the method B3LYP/6-31G**. ² Present work.

Rationalization of the Observed First Electronic Absorption. The leading NTOs, describing the first allowed electronic transition of 3BDP3Ta, have been computed by two methods (Figure 4). Employing the CAM-B3LYP/6-31G** method, we find that two pairs of NTOs, with weights of 0.70 and 0.19, are required to describe the first electronic transition. This involves mainly one BODIPY unit (Figure 4). Using the HSEH1PBE/6-311G** approach, we also find two NTOs, with weights of 0.77 and 0.22. However, the transition involves two BODIPY units and the intervening thiophene groups. It appears that a charge transfer (CT) takes place from the thiophene groups to the BODIPY units. It is observed that the two methods (CAM-B3LYP/6-31G**, HSEH1PBE/6-311G**) give a rather different picture for the transition. It has been noted that CAM-B3LYP overestimates $|E_{HOMO} - E_{LUMO}|$. This may be due to the fact that the present intra-molecular CT transition (Figure 4) is rather short [34].

Computation of the (hyper)polarizabilities. The CAM-B3LYP/6-31G* method has been employed to compute the dipole moment and the (hyper)polarizabilities of derivatives 3BDP3Ta and 3BDP3Tb, both in the gas phase and in solution (solvent: chloroform, water). This method has been successfully applied for the computation of NLO properties of organic and inorganic derivatives [35,36]. The results are presented in Table 2.

Solvent effect. It is observed that the solvent has a significant effect on all the properties. The hyperpolarizabilities β and γ are those which are most affected by the solvent. Thus, it is observed: $\beta(\text{sol})/\beta(\text{gas}) = 1.8$ and $\gamma(\text{sol})/\gamma(\text{gas}) = 1.94$, where $\beta(\text{sol})$ and $\gamma(\text{sol})$ denote the hyperpolarizability values in solution and $\beta(\text{gas})$ and $\gamma(\text{gas})$ are the corresponding values in the gas phase. A small variation of the basis set (6-31G** and 6-311G**) led to insignificant changes of the L&NLO properties.

In order to study the effect of the solvent polarity, we report computations in the presence of a high polar solvent (water, $\epsilon = 80$) since the nanoparticles will be formed in water. The results are shown in Table 2. It is observed that, although the solvent's polarity is substantially increased (c.a 94%), the optical and electrical response properties of both molecules are slightly affected. For example, it is seen that, for the optical response properties of 3BDP3Ta, $\alpha(\text{wat}) = 1.1 \alpha(\text{chloroform})$, $\beta(\text{wat}) = 1.2 \beta(\text{chloroform})$, where α , β , denote the average pol/ty and first hyperpolarizability (CAM-B3LYP/6-311G**), respectively. As far as concerns about the optical absorption of 3BDP3Ta, $\lambda(\text{wat})$ is slightly red shifted, compared with that computed within chloroform. Similar trends are observed for the 3BDP3Tb derivative.

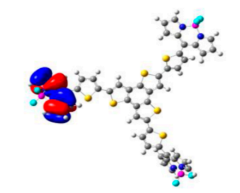
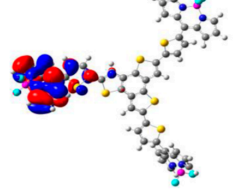
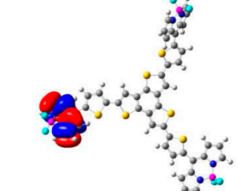
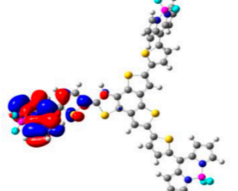
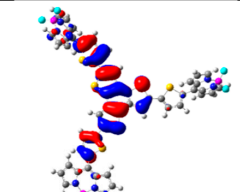
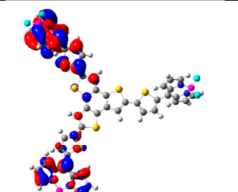
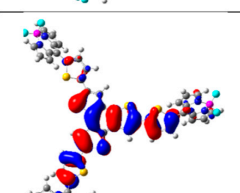
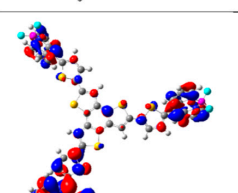
	Hole	Electron	Weight
CAM-B3LYP/6-31G**			0.70
			0.19
HSEH1PBE/6-311G**			0.77
			0.22

Figure 4. The leading NTOs and their weights, describing the first allowed electronic transition of 3BDP3Ta, computed with two methods. Red and blue colors depict positive and negative regions of the orbitals, respectively.

Table 2. The dipole moment (a.u.), (hyper)polarizabilities (a.u), the excitation energy (E_{exc} , eV), the absorption wavelength (λ , nm) of the first electronic allowed transition and the total energy (Hartrees). All the properties were computed at the gas phase optimized geometry (B3LYP/6-31G**).

Molecule	μ	α	β	$\gamma (\times 10^6)$	E_{exc}/λ	E_{tot}
3BDP3Ta						
G.P. ¹	1.1603	962.53	16,053	2.713		-5350.7473^9
Sol. ²	1.4783	1193.43	28,903	5.253	2.78/445.5 ³	
	1.4734	1253.94	31,534	5.774		
	(0.114) ^{4,7}	(1524.4) ^{4,7}	(17,300) ^{4,7}	(10.7) ^{4,7}	2.18/569.4 ⁵	
	1.4675	1371.15	72,505	19.25	2.23/556.8 ⁶	
	(0.108) ^{5,7}	(1699.6) ^{5,7}	(41,700) ^{5,7}	(34.9) ^{5,7}	2.10/590.0 ^{5,11}	
	(0.117) ^{7,8}	(1506.9) ^{7,8}	(15,400) ^{7,8}	(8.5) ^{7,8}		
Exp. ¹⁰	1.633 ^{4,11}	1390.7 ^{4,11}	3685 ^{4,11}		520	
3BDP3Tb						
G.P. ¹						-5350.7514^9
Sol. ^{2,3}	0.095	1201.5	400	5.88	2.78/446.0 ³	
	0.114 ^{3,11}	1326.2 ^{4,11}	577 ^{4,11}		2.15/576.0 ⁵	
					2.08/597.0 ^{5,11}	
Exp. ¹⁰					520	

¹ Properties computed in the gas phase. ² Properties calculated in the presence of the solvent (chloroform). ³ Method: CAM-B3LYP/6-31G**. ⁴ Method: CAM-B3LYP/6-311G**. ⁵ Method: HSEH1PBE/6-311G**. ⁶ Method: B3PW91/6-311G**. ⁷ In a square bracket, the x-component of the property is given. ⁸ Method: MP2/6-311G**. ⁹ Method: B3LYP/6-31G**. $E_{\text{tot}} = E_{\text{el}} + E_{\text{zpv}}$, where E_{el} is the electronic energy and E_{zpv} is the zero-point vibrational averaging correction. ¹⁰ Present work. ¹¹ Solvent: Water.

In terms of a comparison of the properties, $p = \alpha_{xx}$, β_{xxx} , and γ_{xxxx} , computed with the CAM-B3LYP/6-311G* method with those calculated with the MP2/6-311G* technique shows the adequacy of the former for the computation of L&NLO optical properties of the 3BDP3Ta/b derivatives. It is observed that, for 3BDP3Ta, the ratio: $p(\text{MP2})/p(\text{CAMB3LYP}) = 0.99, 0.89,$ and 0.79 , for the polarizability, first and second hyperpolarizability component, respectively. By employing the HSEH1PBE functional, the ratio $p(\text{MP2})/p(\text{HSEH1PBE})$ takes the values of $0.89, 0.37,$ and 0.24 for $\alpha_{xx}, \beta_{xxx},$ and γ_{xxxx} , respectively.

We have also computed the properties of two configurations of 3BDP3T (Figure 3). The first (3BDP3Ta) has the sulfur atoms of thiophenes in a cis arrangement (3BDP3Ta) and the second (3BDP3Tb) in trans. In derivative 3BDP3Tb, the conformation, where the sulfur atoms of thiophenes, are in a trans position that lies lower (2.6 kcal/mol) than the corresponding conformation, where the sulfur atoms of thiophenes are in a cis position (3BDP3Ta). This structural change has a very significant effect on the dipole moment (μ) and the first hyperpolarizability (β).

$$\mu(\text{cis})/\mu(\text{trans}) = 15.6 \text{ and } \beta(\text{cis})/\beta(\text{trans}) = 7.2 \quad (9)$$

This finding highlights the importance of these properties as probes of small differences in the molecular structure. A modest effect is observed for the polarizability and the second hyperpolarizability, while both isomers have practically the same E_{exc} .

In order to further explain, qualitatively, the noticeable difference on β , due to cis and trans arrangement of thiophenes (3BDP3Ta, 3BDP3Tb), the density of the first hyperpolarizability, β , has been computed. This property has been successfully used to explain NLO property differences, resulting by structural changes [35,36]. Only the diagonal component, β_{xxx} , of the density (Figure 5) is reported and analyzed, since it was found that the electronic β_{xxx} value is affected more upon the conformational change (Figure 3), that is $\Delta\beta_{xxx}(3\text{BDP3Ta}-3\text{BDP3Tb}) = 37,891$ a.u. (CAMB3LYP/6-31G**). Therefore, the β_{xxx} density differences are expected to reveal the origin of the noticeable alteration of the β value, upon the conformational change. The computed densities for 3BDP3Ta, 3BDP3Tb are depicted in Figure 5. The Multiwfn software was used.

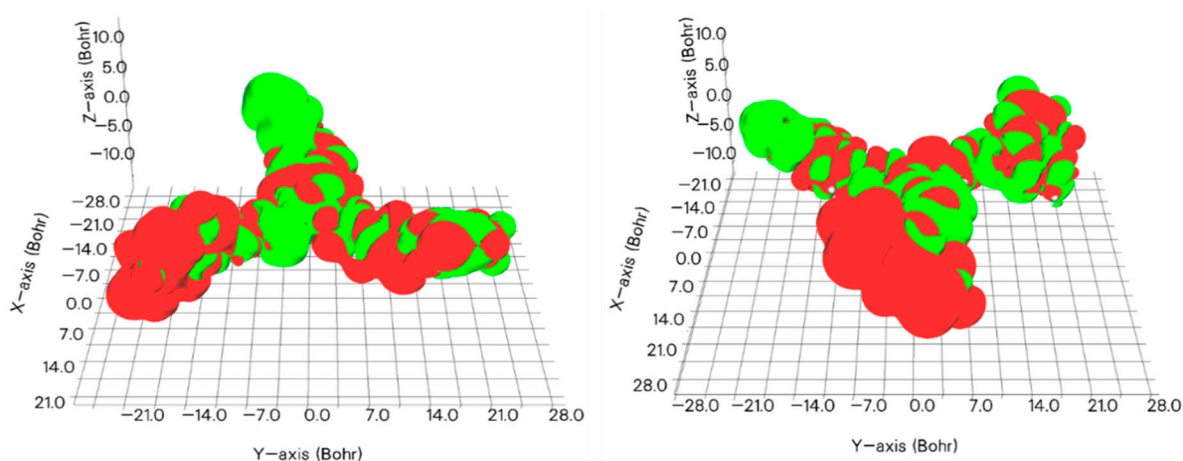


Figure 5. Plots of first hyperpolarizability density $-x\rho_{xx}^{(2)}$ of 3BDP3Ta (left) and 3BDP3Tb (right) derivatives, computed with (U)CAM-B3LYP/6-31G**. A green and red color depict positive and negative contributions, respectively. The first hyperpolarizability densities are represented with contour values of ± 1.0 a.u.

It is observed that, for 3BDP3Ta (Figures 3 and 5), the positive contribution exceeds the corresponding negative one, resulting in a positive β_{xxx} value (15,800 a.u.). Upon changing the positions of thiophenes (cis-trans), the negative contribution to β_{xxx} density is increased, especially in the periphery of the core, thus, changing the sign of the β_{xxx} value ($-22,011$ a.u.).

Comparison of BODIPY with NO₂ and CN. The effect of BODIPY, as an electron acceptor, on the L&NLO properties has been checked by comparing the performance of BODIPY with that of NO₂ and CN, which are known to be very efficient electron acceptors (Figure 6) [33].

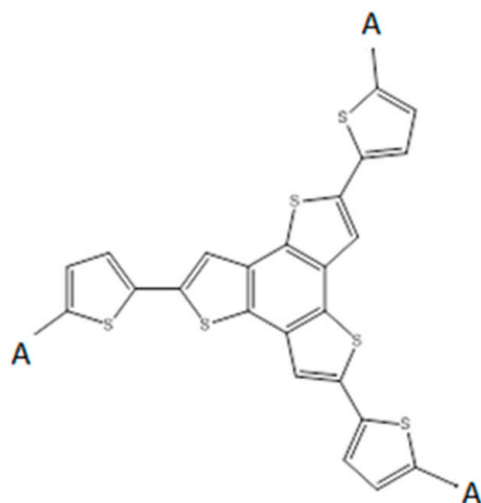


Figure 6. The structure of derivative 1, used for the study of the effect of acceptor, A, where A = BOBIPY, NO₂, and CN.

The results of Table 3 show that $\mu(\text{CN}) > \mu(\text{NO}_2) > \mu(\text{BODIPY})$, but $P(\text{BODIPY}) > P(\text{NO}_2) > P(\text{CN})$, where $p = \alpha, \beta, \text{ or } \gamma$. In fact, BODIPY as an electron acceptor, leads to a much larger $\alpha, \beta, \text{ or } \gamma$ in comparison with NO₂ or CN. This is a very useful finding, since large NLO properties and their tuning are required for many applications (e.g., optoelectronic technologies, optical switching, and telecommunications) [37,38].

Table 3. The dipole moment (a.u.) (hyper)polarizabilities (a.u.), the energy of the HOMO and LUMO, E_{HOMO} and E_{LUMO} , respectively the $E_{\text{HOMO}} - E_{\text{LUMO}}$ gap the excitation energy (E_{exc} ; eV) the absorption wavelength (λ ; nm) of the first electronic allowed transition of 1a with a series of acceptor groups (A). All values are given in a.u.

Molecule ¹ /A	μ ²	α ²	β ²	$\gamma (\times 10^6)$ ²	E_{HOMO} ³	E_{LUMO} ³	$\frac{ E_{\text{HOMO}} - E_{\text{LUMO}} }{3}$	E_{exc}/λ ³
Bodipy	1.474	1193	2890	5.25	−0.215	−0.132	0.083	2.18/569.4
NO ₂	1.561	656	1625	2.54	−0.225	−0.127	0.098	2.62/473
CN	1.629	632	636	1.57	−0.219	−0.104	0.115	3.09/400.5

¹ The geometry, which was employed for the computation of the properties, was optimized at the gas phase with B3LYP/6-31G**, method:

² The properties were computed with CAM-B3LYP/6-31G**, in the presence of the solvent (chloroform), ³ Method: HSEH1PBE/6-311G**, solvent: chloroform.

It is also observed that the type of the acceptor tunes the $|H - L| (= |E_{\text{HOMO}} - E_{\text{LUMO}}|)$ and transition energy, E_{exc} . It was found that $|H - L|(\text{CN}) > |H - L|(\text{NO}_2) > |H - L|(\text{BODIPY})$ and $E_{\text{exc}}(\text{CN}) > E_{\text{exc}}(\text{NO}_2) > E_{\text{exc}}(\text{BODIPY})$. The latter agrees with the observed alteration of the absorption wavelength, λ , of the three acceptors. For example, λ is 569 and 400 nm for BODIPY and CN, respectively.

3.3. Preparation of Nanoparticles

In this work, we prepared 3BDP3T nanoparticles with the encapsulation method. From the three independent DLS measurements, the aqueous nanoparticles show to exhibit a unimodal size distribution with a hydrodynamic diameter of 123.53 ± 0.38 nm (Figure 7), which reflect the reproducibility of the hydrodynamic diameter and the FWHM of the nanoparticle's distribution. Simultaneously with the DLS measurements, the zeta potential of the nanoparticles was measured. The prepared aqueous nanoparticles exhibit a substan-

tial and negative zeta potential of -8.99mV , which is higher than -25 mV . It is well-known that colloidal systems with a zeta potential value of -25 mV or lower (i.e., more negative) exhibit a long-term colloidal stability [39]. The origin of a negative zeta potential has been addressed in previous studies [40] and it is attributed to oxidative defects on the surface of the nanoparticles or to the presence of the π -polarizations of the organic material rings that enable stronger attractive Van der Waals forces and hydrophobic interactions. Therefore, when the organic material is encapsulated inside the amphiphilic copolymer, those interactions are minimized, resulting in lower zeta potential values.

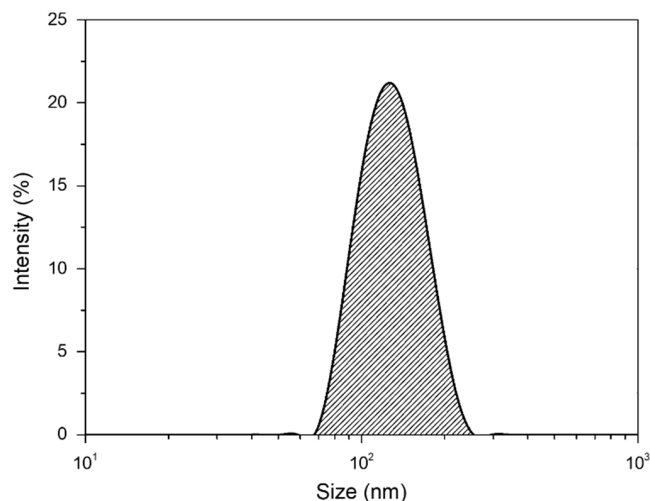


Figure 7. Size distribution of aqueous 3BDP3T nanoparticles prepared via the encapsulation method determined by DLS measurement.

Figure 8 present the UV-Vis absorption and fluorescence spectra of the 3BDP3T-based nanoparticles. An intense absorption peak with λ_{max} at 515 nm and a photoluminescence (PL) with λ_{max} at 642 nm and a shoulder at 752 nm are recorded.

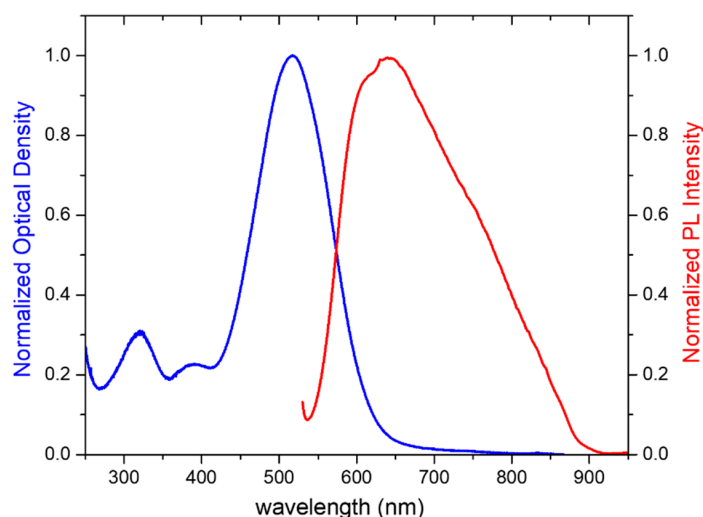


Figure 8. Absorption and photoluminescence spectra of 3BDP3T nanoparticles.

While the absorption maximum of 3BDP3T-based nanoparticles is slightly blue-shifted by 5 nm versus the corresponding 3BDP3T in the THF solution. The PL maximum peaks are significantly red-shifted by 12 nm and 72 nm, respectively. The aqueous 3BDP3T nanoparticles display PL at the far-red and NIR with a PLQY of 0.021 ± 0.003 , which is slightly reduced versus the PLQY of the 3BDP3T in the THF solution, showing that this fabrication methodology for the specific 3BDP3T maintains the PLQY unaltered.

4. Conclusions

In this work, the successful synthesis and properties characterization of a new organic electronic material consisting of three BODIPY dyes at the periphery of the benzo[1,2-*b*:3,4-*b'*:5,6-*b''*]trithiophene (3BDP3T) is presented for the first time. Until now, the development of organic materials with three BODIPYs as substituents is limited and their properties are not fully resolved. We manage to prepare 3BDP3T-based aqueous nanoparticles by utilizing the encapsulation method and study its optical properties toward its application as far-red to near infrared (NIR) dye probe for fluorescent optical imaging. The aqueous 3BDP3T nanoparticles display PL at the far-red and NIR with a PLQY of 0.021 ± 0.003 , which is slightly reduced versus the PLQY of the 3BDP3T in the THF solution, showing that this fabrication methodology for the specific 3BDP3T maintains the PLQY unaltered. From the theoretical study, the main points emerging are the following. The best E_{HOMO} has been computed by PBE1PBE/6-31G** and B3PW91/6-311G**. The best E_{LUMO} has been calculated by HSEH1PBE/6-311G** and B3PW91/6-311G**. The CAM-B3LYP and B3LYP functionals as well as the MP2 method overestimate the $E_{HOMO} - E_{LUMO}$ gap. The best $E_{HOMO} - E_{LUMO}$ gap has been computed by HSEH1PBE/6-311G**. The CAM-B3LYP/6-31G** method provided satisfactory L&NLO properties, as a comparison with the MP2 method has shown. In derivative 3BDP3Tb, the conformation, where the sulfur atoms of thiophenes are in a trans position, lies lower (2.6 kcal/mol) than the corresponding conformation, where the sulfur atoms of thiophenes are in a cis position (3BDP3Tb). This structural change imposes noticeable alterations to μ and β , in contrast to α , γ , and E_{exc} , where the effect of the structure is of less importance. The effect of the structure to β was further investigated by analyzing the first hyper-polarizability density [41]. We have employed two methods to rationalize the observed first absorption of 3BDP3Ta. Both methods give two pairs of NTOs for the description of the first electronic transition. The HSEH1PBE/6-311G** method predicts a transition that involves two BODIPY units and the intervening thiophene groups. Comparison of the BODIPY electron acceptor with other known groups revealed its significant efficiency in tuning the L&NLO response properties of 3BDP3T.

Author Contributions: Conceptualization, C.L.C., V.G.G., A.D.-S. and A.A.; methodology, A.A., A.D.N. and P.K.; data curation, B.M.S., A.A., A.P., M.G.S. and A.S.; writing—original draft preparation, A.D.N., A.A., B.M.S. and C.L.C.; writing—review and editing, all; supervision, C.L.C.; funding acquisition, A.D.-S. and V.G.G. All authors have read and agreed to the published version of the manuscript.

Funding: This research received no external funding.

Acknowledgments: This work was funded by the Helmholtz European partnering program for the cooperation between the German Cancer Research Center (DKFZ) and the National Hellenic Research Foundation (NHRF) to build the Athens Comprehensive Cancer Center (ACCC). In addition, this project has received funding from the European Community's Seventh Framework Programme (FP7/2007–2013) under the Grant Agreements n° 607585 project OSNIRO.

Conflicts of Interest: The authors declare no conflict of interest.

References

1. Yan, C.; Barlow, S.; Wang, Z.; Yan, H.; Jen, A.K.-Y.; Marder, S.R.; Zhan, X. Non-fullerene acceptors for organic solar cells. *Nat. Rev. Mater.* **2018**, *3*, 18003. [CrossRef]
2. Zhang, J.; Tan, H.S.; Guo, X.; Facchetti, A.; Yan, H. Material insights and challenges for non-fullerene organic solar cells based on small molecular acceptors. *Nat. Energy* **2018**, *3*, 720–731. [CrossRef]
3. Hou, J.; Inganäs, O.; Friend, R.H.; Gao, F. Organic solar cells based on non-fullerene acceptors. *Nat. Mater.* **2018**, *17*, 119–128. [CrossRef]
4. Cheng, P.; Li, G.; Zhan, X.; Yang, Y. Next-generation organic photovoltaics based on non-fullerene acceptors. *Nat. Photon.* **2018**, *12*, 131–142. [CrossRef]
5. Nowak-Król, A.; Wagener, R.; Kraus, F.; Mishra, A.; Bäuerle, P.; Würthner, F. Modulation of Band Gap and P-: Versus n-Semiconductor Character of ADA Dyes by Core and Acceptor Group Variation. *Org. Chem. Front.* **2016**, *3*, 545–555. [CrossRef]

6. Wadsworth, A.; Moser, M.; Marks, A.; Little, M.S.; Gasparini, N.; Brabec, C.J.; Baran, D.; McCulloch, I. Critical review of the molecular design progress in non-fullerene electron acceptors towards commercially viable organic solar cells. *Chem. Soc. Rev.* **2019**, *48*, 1596–1625. [[CrossRef](#)]
7. Squeo, B.M.; Gregoriou, V.G.; Avgeropoulos, A.; Baysec, S.; Allard, S.; Scherf, U.; Chochos, C.L. BODIPY-based Polymeric Dyes as Emerging Horizon Materials for Biological Sensing and Organic Electronic Applications. *Prog. Polym. Sci.* **2017**, *71*, 26–52. [[CrossRef](#)]
8. Loudet, A.; Burgess, K. BODIPY Dyes and Their Derivatives: Syntheses and Spectroscopic Properties. *Chem. Rev.* **2007**, *107*, 4891–4932. [[CrossRef](#)]
9. Boens, N.; Leen, V.; Dehaen, W. Fluorescent Indicators Based on BODIPY. *Chem. Soc. Rev.* **2012**, *41*, 1130–1172. [[CrossRef](#)]
10. Zampetti, A.; Minotto, A.; Squeo, B.M.; Gregoriou, V.G.; Allard, S.; Scherf, U.; Chochos, C.L.; Cacialli, F. Highly Efficient Solid-State Near-Infrared Organic Light-Emitting Diodes Incorporating A-D-A Dyes Based on α, β -Unsubstituted “BODIPY” Moieties. *Sci. Rep.* **2017**, *7*, 1–7. [[CrossRef](#)]
11. Treibs, A.; Kreuzer, F.-H. Difluoroboryl-Komplexe von Di-Und Tripyrrylmethenen. *Justus Liebigs Ann. Chem.* **1968**, *718*, 208–223. [[CrossRef](#)]
12. Sathyamoorthi, G.; Boyer, J.H.; Allik, T.H.; Chandra, S. Laser Active Cyanopyromethene- BF₂, Corn Plexes. *Heteroat. Chem.* **1994**, *5*, 403–407. [[CrossRef](#)]
13. Pavlopoulos, T.G.; Shah, M.; Boyer, J.H. Laser Action from a Tetramethylpyromethene-BF₂ Complex. *Appl. Opt.* **1988**, *27*, 4998. [[CrossRef](#)]
14. Wang, D.; Miyamoto, R.; Shiraishi, Y.; Hirai, T. BODIPY-Conjugated Thermoresponsive Copolymer as a Fluorescent Thermometer Based on Polymer Microviscosity. *Langmuir* **2009**, *25*, 13176–13182. [[CrossRef](#)]
15. Rosenthal, J.; Lippard, S.J. Direct Detection of Nitroxyl in Aqueous Solution Using a Tripodal Copper(II) BODIPY Complex. *J. Am. Chem. Soc.* **2010**, *132*, 5536–5537. [[CrossRef](#)]
16. Lee, C.Y.; Hupp, J.T. Dye Sensitized Solar Cells: TiO₂ Sensitization with a Bodipy-Porphyrin Antenna System. *Langmuir* **2010**, *26*, 3760–3765. [[CrossRef](#)]
17. Godoy, J.; Vives, G.; Tour, J.M. Synthesis of Highly Fluorescent BODIPY-Based Nanocars. *Org. Lett.* **2010**, *12*, 1464–1467. [[CrossRef](#)]
18. Terai, T.; Nagano, T. Fluorescent probes for bioimaging applications. *Curr. Opin. Chem. Biol.* **2008**, *12*, 515–521. [[CrossRef](#)]
19. Ulrich, G.; Ziessel, R.; Harriman, A. The Chemistry of Fluorescent Bodipy Dyes: Versatility Unsurpassed. *Angew. Chem. Int. Ed.* **2008**, *47*, 1184–1201. [[CrossRef](#)]
20. Carvalho, P.M.; Felício, M.R.; Santos, N.C.; Gonçalves, S.; Domingues, M.M. Application of Light Scattering Techniques to Nanoparticle Characterization and Development. *Front. Chem.* **2018**, *6*, 1–17. [[CrossRef](#)]
21. Demas, J.N.; Crosby, G.A. The measurement of Photoluminescence Quantum Yields. *J. Chem. Phys.* **1971**, *75*, 991.
22. Biczók, L.; Bérces, T.; Márta, F. Substituent, Solvent, and Temperature Effect on Radiative and Nonradiative Processes of Singlet Excited Fluorenone Derivatives. *J. Phys. Chem.* **1993**, *97*, 8895–8899. [[CrossRef](#)]
23. Fries, F.; Reineke, S. Statistical Treatment of Photoluminescence Quantum Yield Measurements. *Sci. Rep.* **2019**, *9*, 1–6. [[CrossRef](#)] [[PubMed](#)]
24. Cohen, H.D.; Roothaan, C.C.J. Electric Dipole Polarizability of Atoms by the Hartree-Fock Method. I. Theory for Closed-Shell Systems. *J. Chem. Phys.* **1965**, *43*, S34–S39. [[CrossRef](#)]
25. Frisch, M.J.; Trucks, G.W.; Schlegel, H.B.; Scuseria, G.E.; Robb, M.A.; Cheeseman, J.R.; Scalmani, G.; Barone, V.; Mennucci, B.; Petersson, G.A.; et al. *Gaussian 09. Revision A.02*; Gaussian, Inc.: Wallingford, UK, 2009.
26. Tomasi, J.; Mennucci, B.; Cammi, R. Quantum Mechanical Continuum Solvation Models. *Chem. Rev.* **2005**, *105*, 2999–3093. [[CrossRef](#)]
27. Cossi, M.; Barone, V.; Cammi, R.; Tomasi, J. Ab Initio Study of Solvated Molecules: A New Implementation of the Polarizable Continuum Model. *Chem. Phys. Lett.* **1996**, *255*, 327–335. [[CrossRef](#)]
28. Elmowafy, E.M.; Tiboni, M.; Soliman, M.E. *Biocompatibility, Biodegradation and Biomedical Applications of Poly(Lactic Acid)/Poly(Lactic-Co-Glycolic Acid) Micro and Nanoparticles*; Springer: Singapore, 2019; Volume 49.
29. Li, K.; Liu, B. Polymer Encapsulated Conjugated Polymer Nanoparticles for Fluorescence Bioimaging. *J. Mater. Chem.* **2012**, *22*, 1257–1264. [[CrossRef](#)]
30. Ozdemir, M.; Choi, D.; Kwon, G.; Zorlu, Y.; Cosut, B.; Kim, H.; Facchetti, A.; Kim, C.; Usta, H. Solution-Processable BODIPY-Based Small Molecules for Semiconducting Microfibers in Organic Thin-Film Transistors. *ACS Appl. Mater. Interfaces* **2016**, *8*, 14077–14087. [[CrossRef](#)]
31. He, S.; Song, J.; Qu, J.; Cheng, Z. Crucial breakthrough of second near-infrared biological window fluorophores: Design and synthesis toward multimodal imaging and theranostics. *Chem. Soc. Rev.* **2018**, *47*, 4258. [[CrossRef](#)]
32. Martin, R.L. Natural Transition Orbitals. *J. Chem. Phys.* **2003**, *118*, 4775–4777. [[CrossRef](#)]
33. Muller, P. Glossary of terms used in physical organic chemistry. *Pure Appl. Chem.* **1994**, *66*, 1077–1184. [[CrossRef](#)]
34. Huang, S.; Zhang, Q.; Shiota, Y.; Nakagawa, T.; Kuwabara, K.; Yoshizawa, K.; Adachi, C. Computational Prediction for Singlet- and Triplet-Transition Energies of Charge-Transfer Compounds. *J. Chem. Theory Comput.* **2013**, *9*, 3872–3877. [[CrossRef](#)] [[PubMed](#)]
35. Avramopoulos, A.; Otero, N.; Karamanis, P.; Pouchan, C.; Papadopoulos, M.G. A Computational Study of the Interaction and Polarization Effects of Complexes Involving Molecular Graphene and C60 or a Nucleobases. *J. Phys. Chem. A* **2016**, *120*, 284–298. [[CrossRef](#)] [[PubMed](#)]

36. Miletić, T.; Fermi, A.; Orfanos, I.; Avramopoulos, A.; De Leo, F.; Demitri, N.; Bergamini, G.; Ceroni, P.; Papadopoulos, M.G.; Couris, S.; et al. Tailoring Colors by O Annulation of Polycyclic Aromatic Hydrocarbons. *Chem.-A Eur. J.* **2017**, *23*, 2363–2378. [[CrossRef](#)]
37. Sweeney, S.J.; Mukherjee, J. Optoelectronic Devices and Materials. In *Springer Handbook of Electronic and Photonic Materials*; Springer: Berlin/Heidelberg, Germany, 2017.
38. Khalid, M.; Ali, A.; Jawaria, R.; Asghar, M.A.; Asim, S.; Khan, M.U.; Hussain, R.; ur Rehman, M.F.; Ennis, C.J.; Akram, M.S. First principles study of electronic and nonlinearoptical properties of A–D–p–A and D–A–D–p–A configured compounds containing novel quinoline–carbazole derivatives. *RSC Adv.* **2020**, *10*, 22273–22283. [[CrossRef](#)]
39. Gooch, J.W. *Encyclopedic Dictionary of Polymers*; Springer: Berlin/Heidelberg, Germany, 2011.
40. Clifton, S.N.; Beattie, D.A.; Mierczynska-Vasilev, A.; Acres, R.G.; Morgan, A.C.; Kee, T.W. Chemical Defects in the Highly Fluorescent Conjugated Polymer Dots. *Langmuir* **2010**, *26*, 17785–17789. [[CrossRef](#)]
41. Lu, T.; Chen, F. Multiwfn: A Multifunctional Wavefunction Analyzer. *J. Comput. Chem.* **2012**, *33*, 580–592. [[CrossRef](#)]